UDK 620.1:666.762.11:620.3:691.714.018.8
Original scientific article/Izvirni znanstveni članek

ISSN 1580-2949
MTAEC9, 53(4)607(2019)

EFFECT OF Al_2O_3 NANOPARTICLES ON THE TRIBOLOGICAL PROPERTIES OF STAINLESS STEEL

VPLIV DODAJANJA Al_2O_3 NANODELCEV NA TRIBOLOŠKE LASTNOSTI NERJAVNEGA JEKLA

Ana Kračun[1,2], Franc Tehovnik[1], Fevzi Kafexhiu[1], Tadeja Kosec[3], Darja Feizpour[1], Bojan Podgornik[1]

[1]Institute of Metals and Technology, Lepi pot 11, 1000 Ljubljana, Slovenia
[2]Jožef Stefan International Postgraduate School, Jamova cesta 39, 1000 Ljubljana, Slovenia
[3]Slovenian National Building and Civil Engineering Institute, Dimičeva ulica 12, 1000 Ljubljana, Slovenia

Prejem rokopisa – received: 2019-06-03; sprejem za objavo – accepted for publication: 2019-07-08

doi:10.17222/mit.2019.118

Austenitic stainless-steel specimens reinforced with aluminium oxide (Al_2O_3) nanoparticles added in (0.5, 1.0 and 2.5) *w*/% concentrations were produced by a conventional casting route. The produced composite specimens were analysed in terms of microstructural properties and wear resistance. The pin-on-disc testing method was used to study the wear behaviour of the composite at room temperature, including steady-state coefficient of friction, the running-in behaviour and wear resistance. A hardened stainless-steel ball (X47Cr14) with a diameter of 10 mm and hardness of 490 HV1 was used as a loading counter-body, sliding against an investigated disk specimen. Microstructure observations revealed that the concentration and size of the particles have an impact on the distribution of the reinforcement within the matrix as well as on the wear behaviour. The Al_2O_3 particles increased the hardness and consequently led to improved tribological properties of the composites.

Keywords: stainless steel, matrix composites, aluminium oxide, friction, wear

Z metodo konvencionalnega litja je bilo izdelano avstenitno nerjavno jeklo z dodatki nanodelcev aluminijevega oksida (Al_2O_3), v koncentracijah (0.5, 1.0 in 2.5) *w*/%. Izdelane kompozitne vzorce smo analizirali z vidika mikrostrukture in odpornosti proti obrabi. Pri sobni temperaturi so bili izvedeni "pin-on-disc" obrabni testi za preučevanje obnašanja obrabe kompozita in določitve obrabne odpornosti, vključno z beleženjem koeficienta trenja v začetnem in ustaljenem režimu. Kot protitelo smo uporabili kaljeno nerjavno jekleno kroglico (X47Cr14) s premerom 10 mm in trdoto 490 HV1, ki je drsela po preiskovanem vzorcu. Opazili smo, da ima koncentracija in velikost delcev vpliv tako na porazdelitev armature v matrici kot tudi na obrabno obnašanje kompozita. Dodani Al_2O_3 nanodelci so povečali trdoto in posledično izboljšali tribološke lastnosti kompozitov.

Ključne besede: nerjavno jeklo, kompoziti, aluminijev oksid, trenje, obraba

1 INTRODUCTION

Particulate-reinforced metal-matrix composites (MMCs) are well known for their higher specific modulus and strength as well as for their monolithic counterparts.[1] In recent years, the use of iron-based alloys or steels as the matrix material for MMCs has attracted considerable attention from researchers. Fe-based alloys are by the far the most widely used metallic materials because of their low cost and good mechanical properties.

There has been significant research into austenitic stainless-steel-based MMCs, because of the excellent corrosion resistance and workability of the steel matrix. However, austenitic stainless steels have poor wear resistance due to their low hardness.[2] The ceramic reinforcement such as borides, carbides, oxides and nitrides are implemented into steels in order to increase the elastic modulus and to improve the wear resistance, creep and strength. Therefore, these composites can be used for structural applications in the wear industry.[3]

*Corresponding author's e-mail:
anakracun89@gmail.com

In recent years, researches concerning the influence of the different ceramic particulates (TiB_2, TiC, Al_2O_3, Y_2O_3, SiC) on the tribological properties of stainless steels were realized. Also, an improvement in the wear resistance has been observed when intermetallic particles were used as the reinforcement of the steel-matrix composites. The authors focused mainly on studies of the effect of reinforcing phases on the wear resistance, physical, and mechanical properties and the microstructure of the composites.[4,5] For example, Pagounis et al.[6] investigated the abrasion wear behaviour of the steel-matrix composites reinforced with TiC, Al_2O_3 and Cr_3C_2. The results indicate that the incorporation of ceramic particles into austenitic steel matrices can lead to an improvement in the abrasive wear resistance. In the case of composites with stainless-steel matrices, Pagounis at al. have performed a preliminary study on the three-body abrasive behaviour of austenitic (316L) and duplex steels reinforced with Al_2O_3 particles.[6] They pointed out that the addition of a low volume fraction of 10 *x*/% Al_2O_3 particles significantly increases the wear resistance of the steel matrices, without impairing the corrosion properties.[6]

Different factors can affect the wear and friction behavior of MMCs. The basic tribological factors that can control the wear and friction behavior of MMCs can be classified into three categories:[7]

- material factors, such as type of reinforcement, their size, shape, volume fraction and the microstructure of the matrix,
- mechanical or contact factors, such as normal load, sliding velocity and sliding distance,
- physical factors, such as temperature, humidity and environmental conditions.

Two factors have a significant effect on the properties of MMCs. They are (a) distribution of nanoparticles into the metal matrix and (b) de-agglomeration of the nanoparticles. Researchers have demonstrated that by having a good distribution of particles in the metal matrix and avoiding agglomeration of the particles in the matrix, the properties of MMCs can be significantly improved.[7]

There are different routes by which MMCs may be manufactured, and among all the liquid-stat processes are considered to have the most potential for engineering applications in terms of production capacity and cost efficiency. Casting techniques are economical, easier to apply and more convenient for large parts and mass production with regards to other manufacturing techniques. However, it is extremely difficult to obtain a uniform dispersion of ceramic nanoparticles in liquid metals due to the poor wettability and to the difference in specific mass between the ceramic particles and the metal matrix.[5]

The aim of the present work is to produce nanoparticles-reinforced austenitic stainless steel and identify the distribution of particles in the steel matrix that were introduced through a conventional melting and casting method. Furthermore, tribological testing was focused on the influence of different concentrations (0.5, 1.0 and 2.5) *w*/%, sizes (50 and 500) nm and methods of adding Al_2O_3 particles on the friction and wear behaviour of the nanoparticles-reinforced austenitic stainless steel. In terms of methods of adding nanoparticles the focus was on the influence of the dispersion medium CaSi (Ca-30 %, Si-70 %) on the distribution homogeneity of the Al_2O_3 particles.

2 EXPERIMENTAL PART

2.1 Material

Al_2O_3 powder with a mean particle size of 500 nm and 50 nm and austenitic stainless steel (AISI 316) with the chemical composition given in **Table 1** were used as starting materials. The chemical analysis of the material was performed by the means of X-Ray fluorescence (XRF) spectrometry using the Thermo Scientific Niton XL3t GOLDD+ XRF spectrometer.

Austenitic stainless steel has been used for this work, mainly due to its excellent corrosion resistance and distinctive two-phase microstructure of austenite and ferrite. It also belongs to the most used group of stainless steels, also when it comes to loaded parts subjected to sliding and corrosion. They are paramagnetic, have a face-centred cubic lattice and excel with a good combination of hot and cold workability, mechanical properties and corrosion resistance.

Table 1: Chemical composition of the base austenitic stainless steel in mass fractions (*w*/%)

Elements	Si	Mn	Cr	Ni	Cu	Mo	V	C
w/%	0.33	1.24	17.4	10.1	0.36	1.29	0.08	0.02

As reinforcement particles, commercial Al_2O_3 powder from the company US Research Nanomaterials, Inc. with mean particle sizes of 500 nm (**Figure 1a**) and 50 nm (**Figure 1b**) have been used. The Al_2O_3 particles were selected due to their high chemical stability to Fe, good wear resistance and high specific mass. Particularly, it was reported that the wetting angle θ between Al_2O_3 and molten iron alloy is less than 50°, even at high temperatures and in many different types of atmospheres.[8]

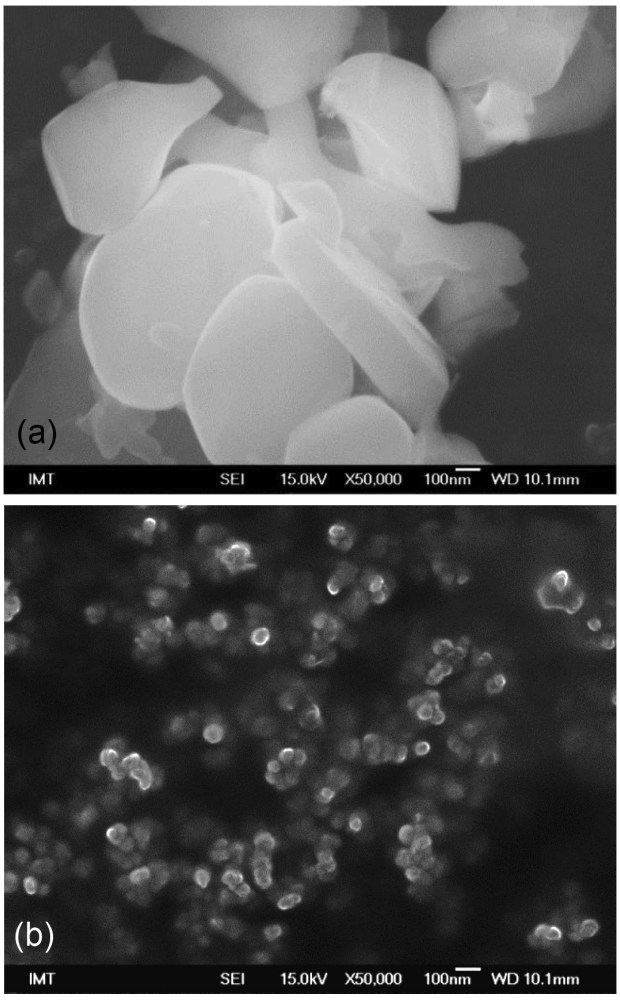

Figure 1: SEI of Al_2O_3 powder with: a) a mean particle size of 500 nm and b) a mean particle size of 50 nm

In the current work commercial CaSi was used as a dispersing agent due to the fact that it is most commonly used as a deoxidant element in steelmaking, and does not cause contamination of the steel melt. In the present case the aim of the CaSi (Ca 30 %, Si 70 %) addition was to control the dispersion (de-agglomeration) and distribution of oxide particles added to the steel melt due to the high reactivity of CaSi.

2.2 Specimens preparation

First, a predefined quantity (20 kg) of base austenitic stainless steel was melted in an induction furnace under normal atmospheric conditions followed by casting in the steel moulds and adding Al_2O_3 nanoparticles. The mass of each cast ingot was 2 kg. In the first set of experiments six different batches were prepared using two different particle sizes (500 nm and 50 nm) and three different concentrations (0.5 *w*/%, 1.0 *w*/% and 2.5 *w*/%) of Al_2O_3. Al_2O_3 powder was wrapped into the aluminium foil, placed into the mould and the molten metal poured over it into the mould. During casting the aluminium foil melts and dissolves in the metal.

The second set of experiments comprised four batches where two different Al_2O_3 particle sizes (500 nm and 50 nm) in concentration of 1.0 *w*/% were used. In two cases Al_2O_3 powder was mixed with the dispersion media, CaSi, in a 1:1 mass ratio and filled into a cast iron tube. For the comparison two additional batches were prepared where only Al_2O_3 powder sealed into a cast iron tube was used. The cast iron tube had a length of 400 mm, outer diameter 12 mm and wall thickness 2 mm, as shown in **Figure 2**. The ends of the tube were sealed with pliers and the molten metal was poured over the iron tube placed into the mould before casting. The iron tube melts and dissolves in the melt.

2.3 Metallographic characterization

The surface of the investigated material was prepared and analysed according to Ref.[9]. The microstructural changes and the dispersion of the ceramic particles in the steel matrix were observed and analysed by scanning electron microscopy (SEM). Samples for microstructure analyses were taken from the middle portion of the cast ingot, with each position comprising 10 randomly selected specimens in order to analyse the homogeneity of the Al_2O_3 particle distribution. Metallographic samples were prepared by grinding using SiC paper, followed by polishing using 1-µm diamond suspension and analysed to reveal the particle distribution. All the specimen surfaces were cleaned with alcohol and dried in hot air.

2.4 Hardness and wear test

The specimens for hardness measurements and tribological tests were taken from the center of the cast ingot at a distance of about 15 mm away from the bottom side. The surface of the samples was prepared according to the technique described in Section 2.3. Vickers hardness measurements of the nanoparticles-reinforced austenitic stainless steel were carried out with an Instron Tukon 2100B machine using a load of 9.807 N (HV1).

Tribological tests were carried out under dry reciprocating sliding contact at room temperature using a TRIBOtechnic Pin-on-Disc TRIBOtester. We selected two sets of test conditions to determine how the material behaves under different loads and sliding speeds. A hardened stainless-steel ball (X47Cr14) with a diameter of 10 mm and hardness of 490 HV1 was used as a loading counter-body, sliding against an investigated disk specimen under a constant load F_n of 1 N or 3 N, corresponding to nominal contact pressures of 470 MPa and 675 MPa, respectively (**Figure 3a**). The sliding amplitude a) was 5 mm, average sliding speed (v_s) was 2 mm/s or 20 mm/s and test duration 300 s or 3000 s, resulting in a total sliding distance of 6 m. In order to establish the test-to-test repeatability of the data, each friction/wear test was repeated three times. The coefficient of friction was measured continuously during the test and the wear

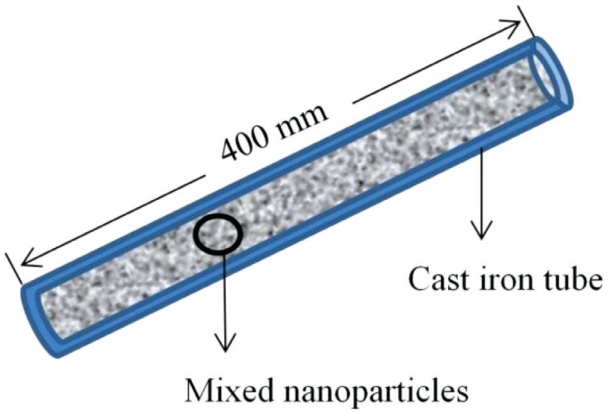

Figure 2: Schematic diagram of a cast iron tube filled with nanoparticles

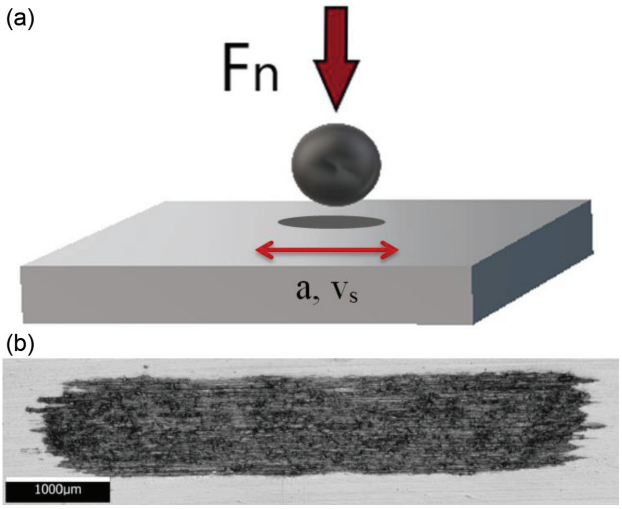

Figure 3: Tribological test: a) Schematic of the ball-on-disk wear test system and b) wear scar

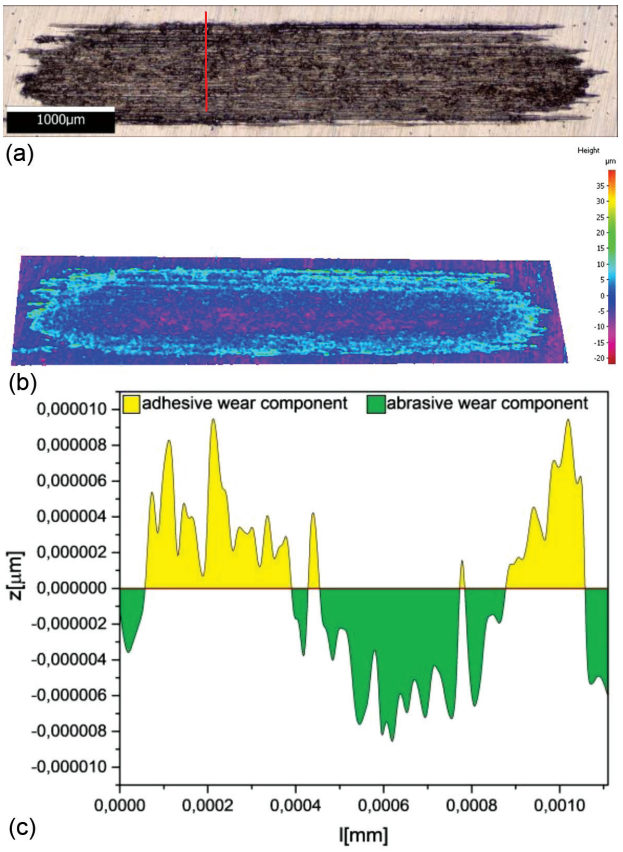

Figure 4: Identification of: a) average cross-section line of the whole wear scar, b) 3D surface profile, c) 2D surface profile

volume determined by the use of a 3D confocal microscope (Alicona Infinite Focus G4) after the completion of the test. An example of a wear scar is shown in **Figure 3b**. In the wear measurements we identify the average cross-section line of the whole wear scar, the 3D surface profile and the 2D surface profile shown in **Figure 4**. For each test, a new ball was used and both specimens washed in high-purity acetone and dried in air prior to testing.

3 RESULTS AND DISCUSSION

3.1 Microstructural characterization

The microstructure studies of Kračun et al.[9] were largely focused on the microstructure of quenched alloys of pure austenitic stainless steel. From the LM micrographs it was established that the matrix consists of a distinctive two-phase microstructure of austenite and δ-ferrites. To show the morphology and size of the Al_2O_3 particles clearly, the etched samples of as-cast austenitic stainless steel and Al_2O_3 particles were examined by SEM, as shown in **Figures 5** to **7**. For a representative analysis of the particle distribution, we took ten images with a scanning electron microscope for each sample taken from the bottom, middle and top portions of the cast piece. In order to conduct the particle analysis

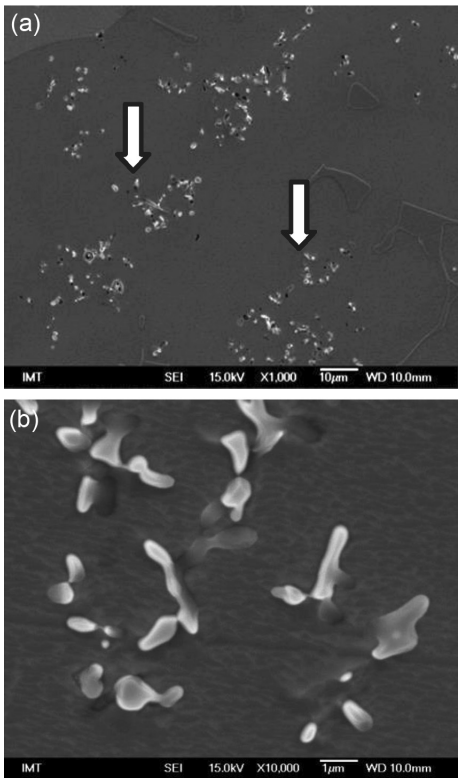

Figure 5: Cast microstructure of austenitic stainless steel at: a) 1,000× magnification and b) 10,000× magnification with 6 % of δ-ferrite and Al_2O_3 (500 nm, 1.0 *w*/%) ultrafine particles (white arrows), without using the CaSi

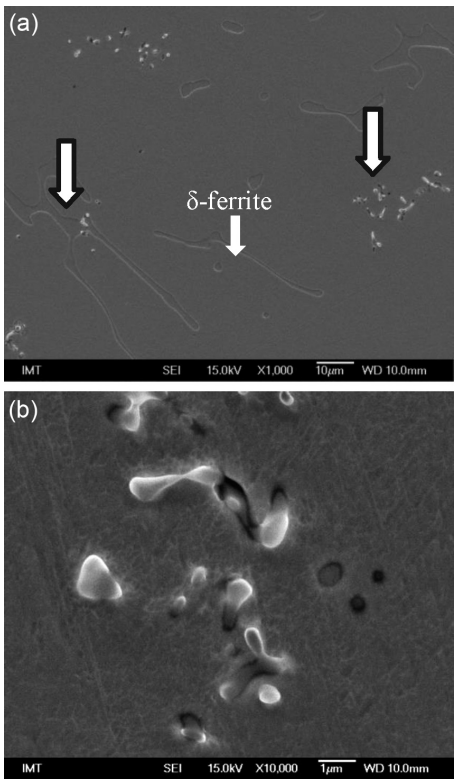

Figure 6: Cast microstructure of austenitic stainless steel at: a) 1,000× magnification and b) 10,000× magnification with 6 % of δ-ferrite (black arrow) and Al_2O_3 (50 nm, 1.0 *w*/%) nanoparticles (white arrows)

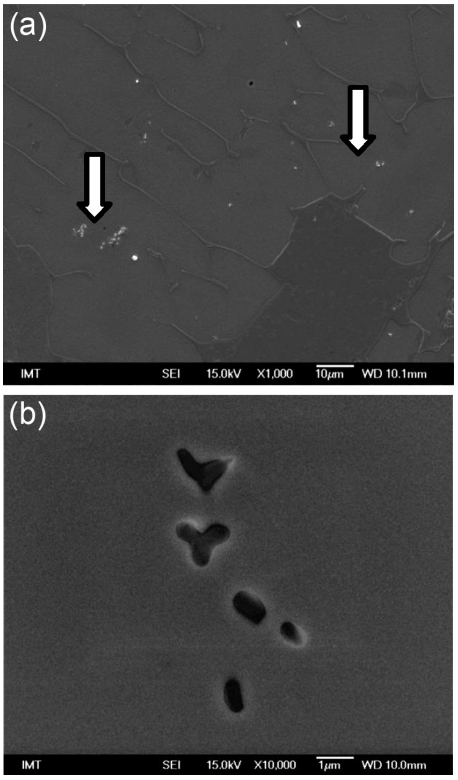

Figure 7: Cast microstructure of austenitic stainless steel at: a) 1,000× magnification and b) 10,000× magnification with 6 % of δ-ferrite and Al_2O_3 (50 nm, 1.0 *w*/%) nanoparticles (white arrows) mixed with CaSi (1.0 *w*/%; Al_2O_3:CaSi = 1:1)

efficiently, all the images were taken at the same magnification (1000×) with similar contrast. It can be seen clearly that the Al_2O_3 particles are incorporated, but non-uniformly distributed in the matrix, with pronounced particle clustering being observed.

Size-dependent analyses also showed that Al_2O_3 powder with a mean particle size of 50 nm is more homogeneously distributed than the 500-nm powder, as indicated by **Figure 7**.

Concentration-dependent analyses showed in **Table 2a** that at the nanoparticle mass fractions of (0.5 and 1.0) *w*/% the number of Al_2O_3 particles per unit area (μm^2) is 0.0087–0.0113 in the case of 50-nm Al_2O_3 particles and 0.0069–0.0073 in the case of 500-nm Al_2O_3 particles. At the nanoparticle mass fractions 2.5 *w*/% the number of Al_2O_3 particles per unit area (μm^2) is in case of 50-nm Al_2O_3 particles 0.0127 and 0.0189 in the case of 500-nm Al_2O_3.

Table 2a: Influence of different concentrations and sizes of Al_2O_3 particles on their distribution, the first set of experiments

Portion of the cast ingot	Weight percent (*w*/%) of Al_2O_3 particles	Number of Al_2O_3 particles per unit area (μm^2)	
		500 nm	50 nm
Middle	0.5	0.0073	0.0113
	1.0	0.0069	0.0087
	2.5	0.0189	0.0127

The particle distribution analyses from the second set of experiments (**Table 2b**) show that the use of a dispersion agent reduces the influence of the particles size (500 nm or 50 nm) on the particle distribution in the steel matrix. It results in a difference in the particles' concentration throughout the ingot being reduced from about 0.01 particles/μm^2 to less than 0.002 particles/μm^2. A concentration-dependent analysis shows in **Table 2b** that at the nanoparticle mass fraction 1.0 *w*/% the number of Al_2O_3 particles per unit area (μm^2) is 0.0154 in the case of 50 nm Al_2O_3 particles and 0.0216 in the case of 500 nm Al_2O_3 particles. At the nanoparticle mass fraction 1.0 *w*/% mixed with CaSi the number of Al_2O_3 particles per unit area (μm^2) is in case of 50-nm Al_2O_3 particles 0.0116 and 0.0093 in the case of 500-nm Al_2O_3.

Table 2b: Influence of different sizes of Al_2O_3 particles and CaSi on the distribution of Al_2O_3 particles (1.0 *w*/%), the second set of experiments

Portion of the cast ingot	Number of Al_2O_3 particles per unit area (μm^2)			
	Al_2O_3 particles (1.0 *w*/%)		Al_2O_3 particles mixed with CaSi (1.0 *w*/%; Al_2O_3:CaSi = 1:1)	
	500 nm	50 nm	500 nm	50 nm
Middle	0.0216	0.0154	0.0093	0.0116

By using CaSi as a dispersion medium and introducing the Al_2O_3/CaSi mixture through a sealed iron tube, reduced particle clustering and a more homogeneous distribution of reinforcement nanoparticles in the steel matrix was obtained, as shown in **Figure 7**. We

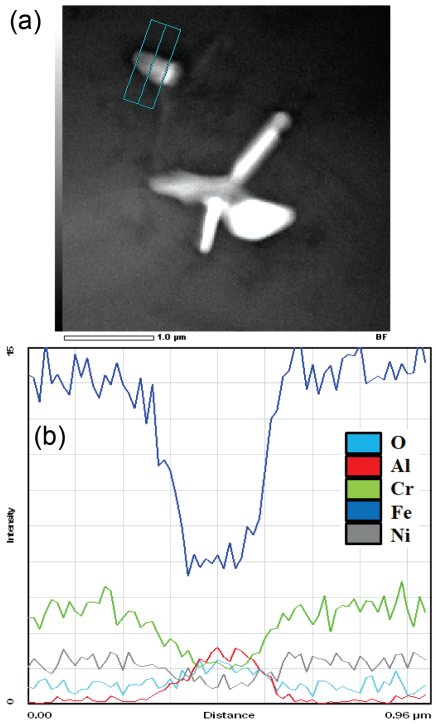

Figure 8: STEM-line profile of Al_2O_3 ultrafine particles (500 nm, 1.0 *w*/%) in the cast microstructure of austenitic stainless steel, without using the CaSi

used CaSi due to the fact that it is highly reactive and is most commonly used as a deoxidant element in steelmaking, and the addition would not cause contamination of the steel melt. During the calcium treatment, the Al_2O_3 inclusions are converted to molten calcium aluminates, which are globular in shape because of the surface-tension effect. The change in inclusion composition and shape is known as the inclusion morphology control. With the addition of CaSi to liquid steel we could control the shape, size and distribution of oxide particles added to the steel melt.

In the context of the microstructural changes' characterization and analysis of the ceramic particles' incorporation into the steel matrix Auger Electron Spectroscopy (AES) and Transmission Electron Microscopy (TEM) were also employed by Kračun et al.[9] With the STEM line-profile analyses in **Figure 8** it was shown that the incorporation and coherent bonding of the Al_2O_3 nanoparticles into the steel matrix was successful. No discontinues at the particle/matrix interface, modification of metal matrix or formation of intermetallic phases could be observed.

3.2 Hardness measurements

Hardness results of the austenitic stainless steel reinforced with (0.5, 1.0, and 2.5) *w*/% Al_2O_3 particles and two different particle sizes (50 nm and 500 nm) are summarised in **Figure 9**. In **Figure 9a** for Al_2O_3 nanoparticles alone and in **Figure 9b** for Al_2O_3 nanoparticles mixed with CaSi. The reference austenitic stainless steel in the as-cast condition showed a hardness of ≈155 HV1. Reinforcement particles' concentration-size dependent analysis shows that austenitic stainless steel reinforced with 1.0 *w*/% Al_2O_3 particles provides the largest hardness increase, especially when using 50-nm-sized particles, followed by (0.5 and 2.5) *w*/%. The austenitic stainless steel with 0.5 *w*/% Al_2O_3 with a mean particles size of 500 nm displays the hardness of about 195 HV1, at 1.0 *w*/% the hardness reaches the maximum value of over 205 HV1, while at 2.5 *w*/% the hardness again decreases to ≈180 HV1. An even higher maximum hardness is obtained when using smaller Al_2O_3 particles of 50 nm. In the case of the austenitic stainless steel reinforced with 0.5 *w*/% of 50-nm-sized Al_2O_3 nanoparticles the hardness is similar to the larger particles case of about 195 HV1. However, as the concentration of 50-nm-sized Al_2O_3 nanoparticles was increased to 1.0 *w*/% a maximum hardness of almost 220 HV1 is reached, as shown in **Figure 9a**. On the other hand, a further increase in the concentration of small nanoparticles (2.5 *w*/%) had the opposite effect, with the hardness being decreased to about 170 HV1.

By mixing Al_2O_3 nanoparticles with the CaSi dispersive medium, which facilitates a more homogeneous and uniform distribution of nanoparticles in the steel matrix an additional increase in the hardness is obtained. In the case of the austenitic stainless steel reinforced with 1.0 *w*/% of 500-nm-sized Al_2O_3 particles the hardness increased from 170 HV1 to about 185 HV1 when adding CaSi to Al_2O_3 powder. Also, in the case of smaller 50-nm-sized Al_2O_3 nanoparticles mixing nanoparticles with the CaSi dispersive medium has similar effect. It increased the hardness of the austenitic stainless steel with 1.0 *w*/% of 50-nm-sized Al_2O_3 nanoparticles from ≈165 HV1 to almost 180 HV1, as shown in **Figure 9b**.

In general, the successful incorporation of the Al_2O_3 nanoparticles was found to increase the hardness of the austenitic stainless steel. Furthermore, the addition of CaSi has a significant effect on the distribution and de-agglomeration of the particles (**Figure 7**), thus modifying the hardness of the material. As shown in **Figure 9b**, for both Al_2O_3 particle sizes the addition of CaSi tends to further increase the austenitic stainless steel's hardness.

3.3 Wear testing results

Figure 10 shows the variation of the coefficient of friction for austenitic stainless steel and investigated reinforced composites, tested for 300 s at a load of 1N and a sliding speed of 20 mm/s. As shown, the coeffi-

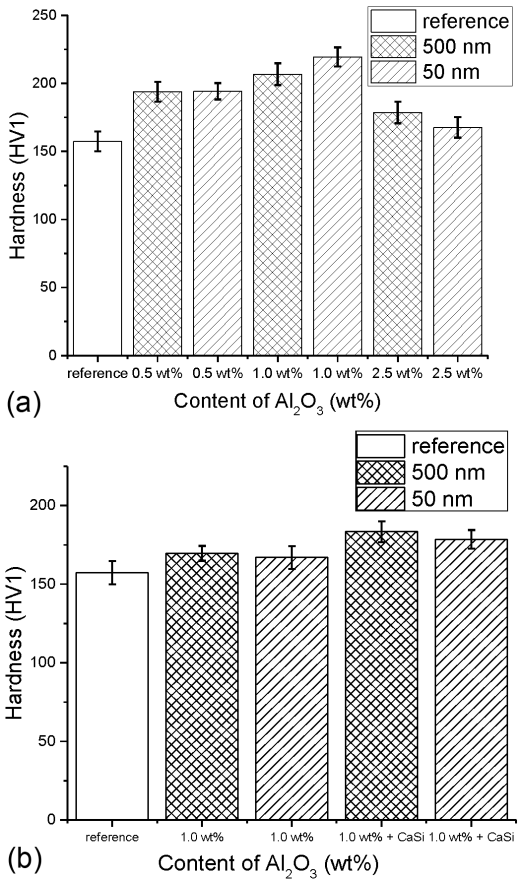

Figure 9: Results of hardness measurements (HV1) for different content of Al_2O_3 particles (*w*/%) and different particle sizes for: a) 1st set of experiments and b) 2nd set of experiments with added CaSi dispersive media

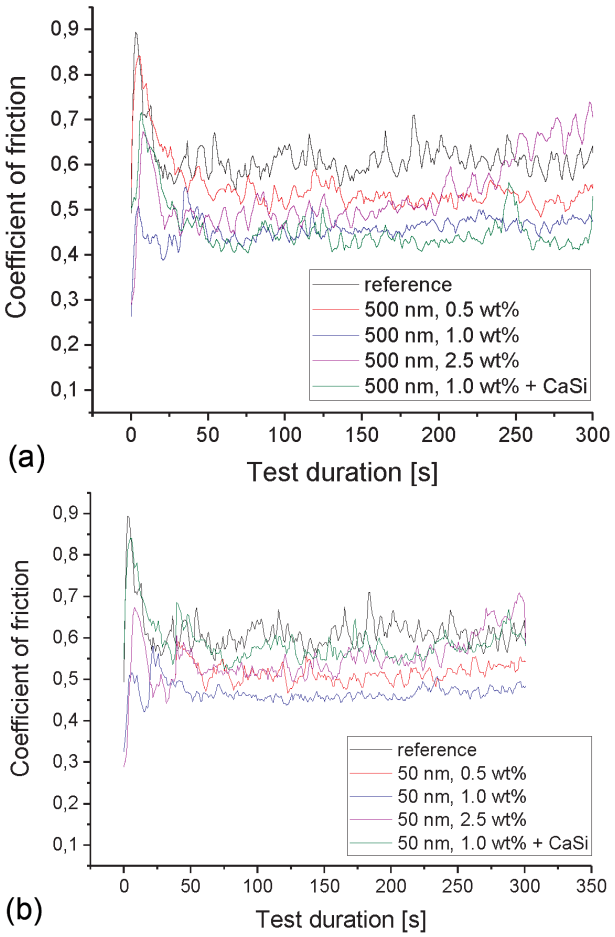

Figure 10: Coefficient-of-friction curves for the reference austenitic stainless steel and investigated composites, tested at load 1 N, sliding speeds 20 mm/s and test time 300 s for: a) Al_2O_3 particles in size 500 nm and b) Al_2O_3 particles in size 50 nm

cient of friction decreases with the addition of Al_2O_3 nanoparticles, reducing the steady-state coefficient of friction for austenitic stainless steel from 0.6 even down to about 0.4. In the case of 500-nm-sized Al_2O_3 particles the lowest and the most stable coefficient of friction of about 0.45 was obtained at 1.0 *w*/% concentration (**Figure 10a**), which is also true for the 50-nm-sized nanoparticles (**Figure 10b**). However, in the case of 500-nm particles the addition of CaSi further improves the friction behaviour of austenitic stainless steel, as shown in **Figure 10a**. The same trends and similar coefficient-of-friction values are observed also for a sliding speed of 2 mm/s and a normal load of 3 N, with the addition of Al_2O_3 particles reducing the coefficient of friction and the lowest and the most stable friction being provided by 500-nm-sized Al_2O_3 particles added in 1.0 *w*/% concentration and CaSi used as a dispersion agent, as shown in **Figure 11.**

Although the variation in coefficient of friction values is not large, it shows a reducing trend when the Al_2O_3 particles are added to the austenitic stainless steel. Moreover, the coefficient of friction depends on the content and size of Al_2O_3 particles, with 500-nm Al_2O_3 particles and 1.0 *w*/% concentration giving the best results, as shown in **Figure 11**.

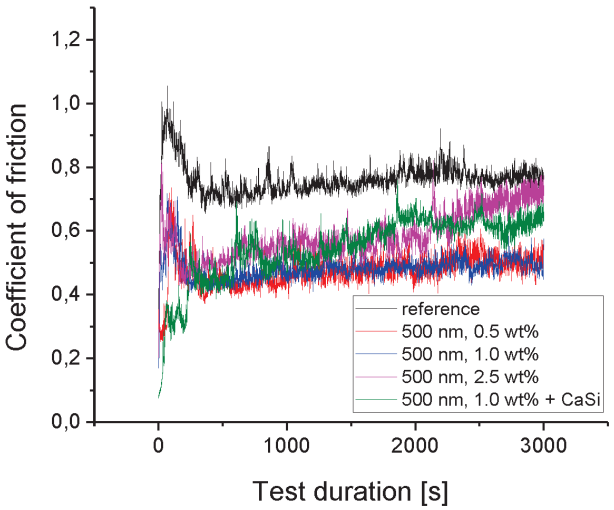

Figure 11: Coefficient-of-friction curves for the reference austenitic stainless steel and investigated composites, tested at load 3 N, sliding speeds 2 mm/s and test time 3000 s

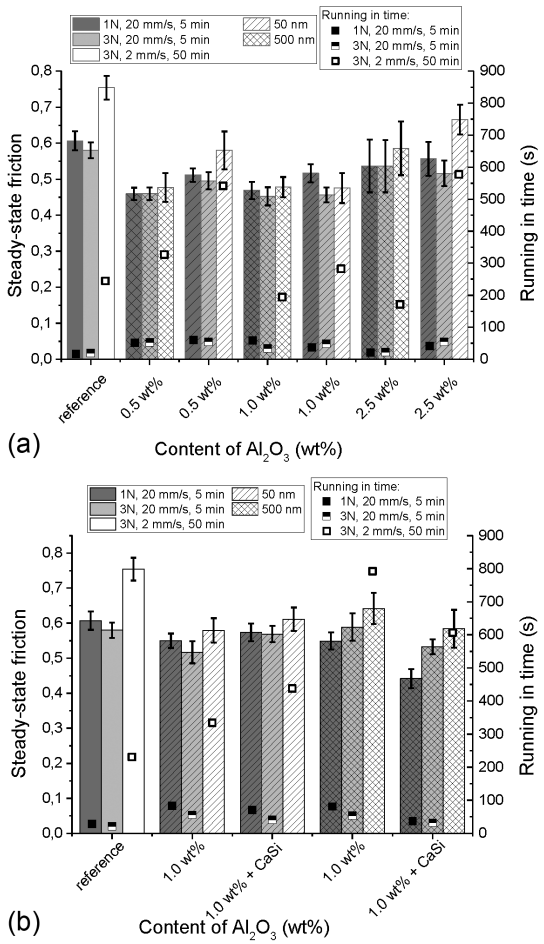

Figure 12: Steady-state coefficient of friction and running-in time for tested composites in samples: a) without CaSi and b) with added CaSi

In **Figure 12** the results for the steady-state coefficient of friction and running-in time required to reach steady-state conditions are shown for different contents of Al_2O_3 particles (*w*/%) and different particle sizes. The error bars in **Figure 12** represent the scatter of three parallel tests. As shown in **Figure 12a**, the best results in the case of Al_2O_3 nano-particles being added without any dispersive media were obtained with 500-nm-sized Al_2O_3 particles added in 2.5 *w*/% concentration. In the case of 500-nm-sized Al_2O_3 particles the lowest steady-state coefficient of friction was obtained and reached in the shortest time; after about 20 s for a high sliding speed (20 mm/s) and after 170 s for a low sliding speed (2 mm/s).

Also in the case of Al_2O_3 nanoparticles being mixed with the CaSi dispersive medium (1:1 ratio), as shown in **Figure 12b**, the best results were obtained in the case of 500-nm Al_2O_3 particles, but this time for a lower concentrations of 1.0 *w*/%. For a high sliding speed (20 mm/s) steady-state conditions were reached after about 35 s. However, for a low sliding speed (2 mm/s) the 50-nm-sized Al_2O_3 nanoparticles gave a faster running-in, with the steady-state conditions being reached after about 400 s.

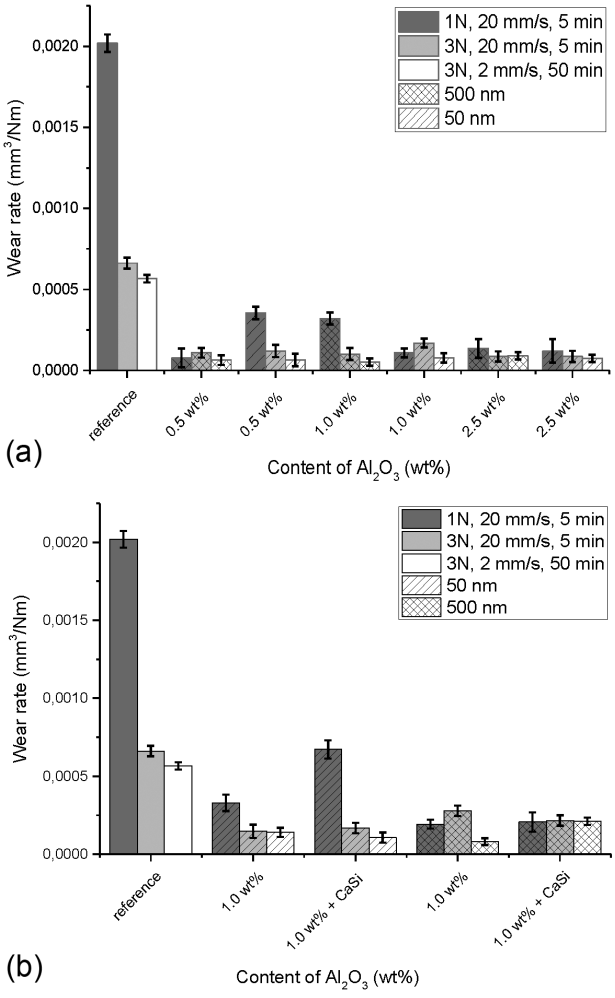

Figure 13: Wear rates as a function of: a) Al_2O_3 particles size and concentration and b) addition of CaSi dispersive media

Figure 13 shows the wear rate *k*, calculated according to eqn. 1 for the investigated composite specimens tested at two different loads (1 N, 3 N) and two sliding speeds (2 mm/s, 20 mm/s).

$$k = \frac{W}{F_N \cdot s} \ [\text{mm}^3/\text{Nm}] \tag{1}$$

where W is the wear volume, F_N is the normal load and s is the sliding distance.

As shown in **Figure 13**, with the addition of Al_2O_3 particles the wear rate of austenitic stainless steel has been reduced by more than an order of magnitude. The wear rate of the reference austenitic stainless steel has been reduced from $2.0 \cdot 10^{-3}$ mm³/Nm down to $0.1–0.4 \cdot 10^{-3}$ mm³/Nm when adding Al_2O_3 reinforcement nanoparticles (**Figure 13a**). It is evident that the Al_2O_3 particles' addition is beneficial in improving the wear resistance of stainless steel due to the high hardness and better wear resistance of the reinforcing Al_2O_3 ceramic particles. Reinforcement particles concentration-size dependent analysis shows that the lowest austenitic stainless-steel wear rate is obtained when reinforced with 0.5 *w*/% Al_2O_3 particles with the mean particles size of 500 nm. In the case of the 50-nm-sized Al_2O_3 particles the best results in terms of low wear rate are obtained when using an Al_2O_3 nanoparticles concentration of 2.5 *w*/%. However, the level of wear is very similar for both particle sizes, especially at higher concentrations ($\geq$ 1.0 *w*/%). On the other hand, the distribution of nanoparticles does not seem to play a role on the austenitic stainless steel wear resistance, regardless of the particles' size and concentration. Either using Al_2O_3 nanoparticles with or without the CaSi dispersive medium results in a very similar wear rate of about $0.25 \cdot 10^{-3}$ mm³/Nm, as shown in **Figure 13b**.

4 CONCLUSIONS

The purpose of this research was to assess the influence of different concentrations, sizes and methods of adding Al_2O_3 particles on the friction and wear behaviour of the nanoparticles-reinforced austenitic stainless steel. Furthermore, we focus on the methods and possibilities of the uniform distribution of the particles within the steel matrix using conventional casting routes. Through a proper insertion method the nanoparticles can be successfully introduced into the metal matrix and improve the wear behaviour and hardness of the stainless steel by using conventional casting routes. The Al_2O_3 nanoparticles were successfully incorporated into the steel matrix with no signs of any intermetallic reactions taking place between the nanoparticles and the steel matrix.

As a result of this work, the major new findings concerning the mechanistic role of additives on the wear behaviour of the stainless steel were:

In general, the incorporation of the Al_2O_3 nanoparticles was found to increase the hardness of the austenitic stainless steel. Furthermore, the addition of CaSi has a significant effect on the distribution and de-agglomeration of the particles, thus modifying the hardness of the material. Reinforcement particles concentration-size dependent analysis shows that austenitic stainless steel reinforced with 1.0 *w*/% Al_2O_3 particles provides the highest hardness increase, especially when using 50-nm-sized particles, followed by (0.5 and 2.5) *w*/%.

In terms of tribological properties the addition of Al_2O_3 nanoparticles reduces steady-state coefficient of friction but leads to a prolonged running-in period. Although the variation in coefficient of friction values is not large, it shows reducing trend when the Al_2O_3 particles are added to the austenitic stainless steel. Moreover, the coefficient of friction depends on the content and size of Al_2O_3 particles, with 500-nm Al_2O_3 particles and 1.0 *w*/% concentration giving the best results, which can be further improved by obtaining a more homogeneous distribution of nanoparticles in the matrix.

Furthermore, by the incorporation of hard and wear-resistant Al_2O_3 ceramic nanoparticles the wear resistance of the austenitic stainless steel has been improved by more than an order of magnitude. Reinforcement particles concentration-size dependent analysis shows that the lowest wear rate of the austenitic stainless steel is obtained when reinforced with larger Al_2O_3 particles (500 nm) but in a lower concentration of 0.5 *w*/%. In the case of 50-nm-sized Al_2O_3 particles a similar level of wear rate is obtained; however, the lowest wear rates are obtained for larger particles concentrations of 2.5 *w*/%. In terms of wear resistance more uniform distribution of nanoparticles, obtained by adding the CaSi dispersive medium, did not show any further improvement.

Acknowledgment

This work was done in the frame of the research programs P2-0050, which is financed by the Slovenian Research Agency. The authors would like to thank Miroslav Pečar, inž. for the help with the AES analysis and dr. Borut Žužek for the hardness measurements.

5 REFERENCES

[1] S. C. Tjong, K. C. Lau, Sliding wear of stainless steel matrix composite reinforced with TiB_2 particles, Mater. Lett., 41 (**1999**) 4, 153–158, 1999, doi:10.1016/S0167-577X(99)00123-8

[2] Z. Ni, Y. Sun, F. Xue, J. Bai, Y. Lu, Microstructure and properties of austenitic stainless steel reinforced with in situ TiC particulate, Mater. Des., 32 (**2011**) 3, 1462–1467, doi:10.1016/j.matdes.2010.08.047

[3] S. Chen, P. Seda, M. Krugla, A. Rijkenberg, High-modulus steels reinforced with ceramic particles through ingot casting process, Mater. Sci. Technol., 32 (**2016**) 10, 992–1003, doi:10.1080/02670836.2015.1104082

[4] F. Akhtar, Ceramic reinforced high modulus steel composites: processing, microstructure and properties, Can. Metall. Q., 53 (**2014**) 3, 253–263, doi:10.1179/1879139514Y.0000000135

[5] B. N. Chawla, Y. Shen, Mechanical behavior of particle reinforced metal matrix composites, Adv. Eng. Mater., 3 (**2001**) 6, 357–370, doi:10.1002/1527-2648(200106)3:6<357:aid-adem357> 3.3.co;2-9

[6] E. Pagounis, V. K. Lindroos, M. Talvitie, Influence of matrix structure on the abrasion wear resistance and toughness of a hot isostatic pressed white iron matrix composite, Metall. Mater. Trans. A, 27 (**1996**), 4183–4191

[7] P. L. Menezes, S. P. Ingole, M. Nosonovsky, S. V. Kailas, M. R. Lovell, Tribology for scientists and engineers: From basics to advanced concepts, Springer, 2013

[8] S.-Y. Cho, J.-H. Lee, Anisotropy of wetting of molten Fe on Al_2O_3 single crystal, Korean J. Mater. Res., 18 (**2018**) 1, 18–21, doi:10.3740/MRSK.2008.18.1.018

[9] A. Kračun, M. Torkar, J. Burja, B. Podgornik, Microscopic characterization and particle distribution in a cast steel matrix composite, Mater. Tehnol., 50 (**2016**) 3, 451–454, doi:10.17222/mit. 2015.310